The Recombination Mediator BRCA2

Architectural Plasticity of Recombination Intermediates Revealed by Single-Molecule Imaging (SFM/TIRF)

Sidhu, Arshdeep; Ristic, Dejan; Sánchez, Humberto; Wyman, C

DOI
10.1016/bs.mie.2017.11.014

Publication date
2018

Document Version
Proof

Published in
Methods in Enzymology

Citation (APA)
Sidhu, A., Ristic, D., Sánchez, H., & Wyman, C. (2018). The Recombination Mediator BRCA2: Architectural Plasticity of Recombination Intermediates Revealed by Single-Molecule Imaging (SFM/TIRF). In M. Spies, & A. Malkova (Eds.), *Methods in Enzymology* (Vol. 600, pp. 347-374). (Methods in Enzymology; Vol. 600). Academic Press. https://doi.org/10.1016/bs.mie.2017.11.014

CHAPTER FOURTEEN

The Recombination Mediator BRCA2: Architectural Plasticity of Recombination Intermediates Revealed by Single-Molecule Imaging (SFM/TIRF)

Arshdeep Sidhu*, Dejan Ristic*, Humberto Sánchez†, Claire Wyman*,1

*Erasmus University Medical Center, Rotterdam, The Netherlands
†Kavli Institute of Nanoscience, Faculty of Applied Sciences, Delft University of Technology, Delft, The Netherlands
1Corresponding author: e-mail address: c.wyman@erasmusmc.nl

Contents

Methods in Enzymology, Volume 600
ISSN 0076-6879
https://doi.org/10.1016/bs.mie.2017.11.014

Abstract

Cellular functions are defined by dynamic assembly, rearrangement, and disassembly of biomolecules to achieve control and specificity. As an example, effective DNA repair is brought about by the concerted action of several DNA processing proteins. Both changes in the structure of individual proteins and in the arrangement of multiple proteins together (referred to here as architecture) are inherent to biological function. These dynamic changes are exemplified in the breast cancer susceptibility protein 2 (BRCA2). BRCA2 is a DNA repair protein that undergoes changes in its own structure and affects changes in molecular architecture with partners during homologous recombination (HR) repair of DNA double strand breaks. These challenging features of BRCA2 protein, its size and predicted stretches of intrinsically disordered regions, have made it difficult to determine the structural consequences and mechanistic importance of interactions between full-length BRCA2 with RAD51 and other HR proteins. In this chapter, we describe scanning force microscopy (SFM)-based approaches to study DNA–protein complexes involved in HR, the architectural plasticity of full-length BRCA2, and the dynamic reorganization of these molecular components associated with essential steps of HR.

1. INTRODUCTION

DNA lesions caused by a number of extrinsic and intrinsic factors challenge genomic integrity on a daily basis. DNA double strand DNA breaks (DSBs) are potentially one of the most toxic DNA lesions. Incorrect repair of DSBs can result in point mutations, small deletion mutations, or more dramatically in chromosomal translocations, which are common precursors to neoplastic transformation. Most of the incurred DSBs are repaired by homologous recombination (HR) or nonhomologous end joining repair pathways. The choice of repair pathway depends on the phase of cell cycle and the availability of a homologous chromosome for repair. HR repair is essential for supporting replication and is the most accurate mechanism for repair of DSBs (Mehta & Haber, 2014; van Gent, Hoeijmakers, & Kanaar, 2001).

HR repair requires the coordinated action of many DNA repair proteins including RAD50, Mre11, NBS1, RPA, RAD51 (and its paralogs), RAD52, BRCA1, BRCA2, DSS1, and RAD54. Some of these proteins, like MRE11, RAD51, have catalytic function in the repair process while others, like NBS1, RPA, BRCA2, have regulatory or structural roles (Stracker, Theunissen, Morales, & Petrini, 2004). Precisely coordinated intermolecular protein interactions among these proteins are essential for

maintaining an error-free genome. Detailed understanding of molecular interactions and their structural consequences in HR repair can contribute important insight needed to design new therapeutic strategies and manage pathologies in, for instance, cancers where the role of HR in genomic (in)stability is linked to both causes and cures.

The protein–protein interactions in the HR repair pathways have been studied by a variety of biochemical, structural, biophysical, and single-molecule approaches (Jensen, Carreira, & Kowalczykowski, 2010; Modesti et al., 2007; Sanchez, Kertokalio, van Rossum-Fikkert, Kanaar, & Wyman, 2013; Sanchez et al., 2017; Shahid et al., 2014; Thorslund et al., 2010; Yang et al., 2002; Yang, Li, Fan, Holloman, & Pavletich, 2005). Nevertheless, it remains difficult to define dynamic changes in molecular structure and complex architecture. Although X-ray crystallography and NMR provide atomic resolution, both these techniques require high concentration of protein and are limited by intrinsic structural flexibility of the proteins and architectural variability of the complexes being analyzed. Protein and DNA molecules are nanoscale entities whose molecular interactions can be determined by techniques that visualize single molecules. Single-molecule imaging by scanning force microscopy (SFM) and (cryo-) EM have been used successfully with full-length proteins to reveal nanoscale structures and molecular characteristic of several DNA repair complexes (Sanchez et al., 2013, 2017; Shahid et al., 2014; Thorslund et al., 2010). SFM does not require the class averaging of thousands of single-molecule projections needed in cryo-EM to reconstruct a 3D particle image and therefore reveals structural information on each individual molecule/complex observed. This yields rich information on all conformation of complexes in a mixture and their distributions in variable but defined conditions provide additional information on dynamic arrangement.

SFM imaging is well suited for analysis of conformational flexibility of proteins and architectural variability of their complexes. Recent advances combining fluorescence microscopy with SFM topography significantly broaden the possible applications. Individual protein or DNA components in complex assemblies can be identified and quantified based on signals from fluorescent tags. This can provided essential new information on molecular composition and architecture of multicomponent complexes. This chapter focuses on the SFM-based approaches to study protein–protein and protein–DNA interactions at molecular resolution in the context of HR repair. We introduce methods developed so far to obtain additional information by combining total internal reflection fluorescence (TIRF) microscopy with SFM.

We focus on the breast cancer susceptibility protein 2, BRCA2, to investigate the role of conformational dynamics in interaction with RAD51. BRCA2 is an essential mediator of RAD51, required for localizing RAD51 to sites of DNA damage and exchanging RPA for RAD51 on single-stranded DNA in need of HR repair (Jensen et al., 2010; Kolinjivadi et al., 2017; Prakash, Zhang, Feng, & Jasin, 2015). BRCA2 consists of 3418 amino acids including domains that interact with RAD51, PALB2, DNA, and other partners, but notably also large stretches predicted to be intrinsically disordered regions (IDRs). From a practical point of view, protein purification requires expression in mammalian cells and typically yields are rather low, in the range of micrograms of protein from a liter of culture (Jensen et al., 2010; Sanchez et al., 2017). Given these features BRCA2 is ideally suited for SFM-based studies. A typical SFM imaging experiment requires only tens of microliters volume of sample in standard biochemical buffers at nanogram per microliter concentrations. The images obtained provide nanometer resolution information on shape, size, and volume of the objects in the sample, where volume correlates linearly with molecular mass (Moreno-Herrero et al., 2005; Ratcliff & Erie, 2001; Wyman, Rombel, North, Bustamante, & Kustu, 1997). Thus, single-molecule imaging of proteins and protein complexes by SFM can determine the distribution of conformations and multimerization state of protein in physiologically relevant buffer conditions. TIRF microscopy can be combined with SFM to identify specific proteins in complex structures by fluorescent labels and single-molecule localization. Although technically challenging, combined TIRF–SFM provides richer data and is an exciting advance for studying dynamic multicomponent processes such as HR.

2. ORGANIZATION AND ARCHITECTURAL PLASTICITY OF PROTEIN AND DNA–PROTEIN ASSEMBLIES: SINGLE-MOLECULE SFM IMAGING

SFM imaging, in brief, includes sample deposition onto a substrate, which is then scanned by a sharp tip to generate images. Primary factors that determine the quality of SFM imaging include the sample quality, tip–sample interactions, and substrate. In the following paragraphs we discuss how these three primary factors affect the quality of SFM imaging with respect to the DNA repair complexes we study:

2.1 Sample Quality

For SFM experiments sample quality involves two aspects, *purity* and *concentration*. Purity is important because any material in the sample with a size of a few Angstroms up to 100 nm can severely compromise image quality. Impurities larger than 100 nm impede imaging altogether. Therefore, all the buffers and consumables involved in sample preparation should be "nanoscopically" clean, prepared with pure components, if necessary filtered but not autoclaved. Concentration of the molecules of interest and their affinity for the substrate will determine coverage, density of objects of interest in the images obtained. Ideal sample coverage results in individual molecular species that can be recognized but are not overlapping. The goal is to be able to unambiguously identify molecules/complexes of interest and to have sufficient examples recorded in a reasonable number of scan images (Fig. 1). Coincidental colocalization of, for instance, monomers/dimers due to crowding can appear as potential larger oligomers complicating or preventing analysis of oligomerization (Fig. 1B and C). Normally, about 1–2 ng/μL of protein in the mixture to be deposited is sufficient for imaging. However, when studying protein complexes and interactions, the concentration of the components should be at least a magnitude higher than the affinity of their interaction (K_d), which may then require dilution in the deposition step. Buffer conditions are usually determined by the interactions being studied based on prior biochemical analysis. A range of standard biochemical reactions conditions is suitable for SFM sample preparation allowing deposition of complexes directly from biochemically active conditions.

2.2 Tip–Sample Interaction

SFM imaging modes are categorized based on the extent of tip–sample interaction as contact, tapping, and true noncontact mode. We use almost exclusively tapping mode SFM and refer only to this imaging mode here. One of the unavoidable aspects of tip–sample interactions is convolution of the size of the molecules being imaged and the size and shape of the scanning tip apex. Using standard tips with ~10 nm radius this typically results in exaggerated X–Y dimensions for biomolecules such as DNA (Fuentes-Perez, Dillingham, & Moreno-Herrero, 2013; van Raaij, Segers-Nolten, & Subramaniam, 2006; Yang, Vesenka, & Bustamante, 1996). Short range tip–sample and tip–substrate interactions, attraction and repulsion, result

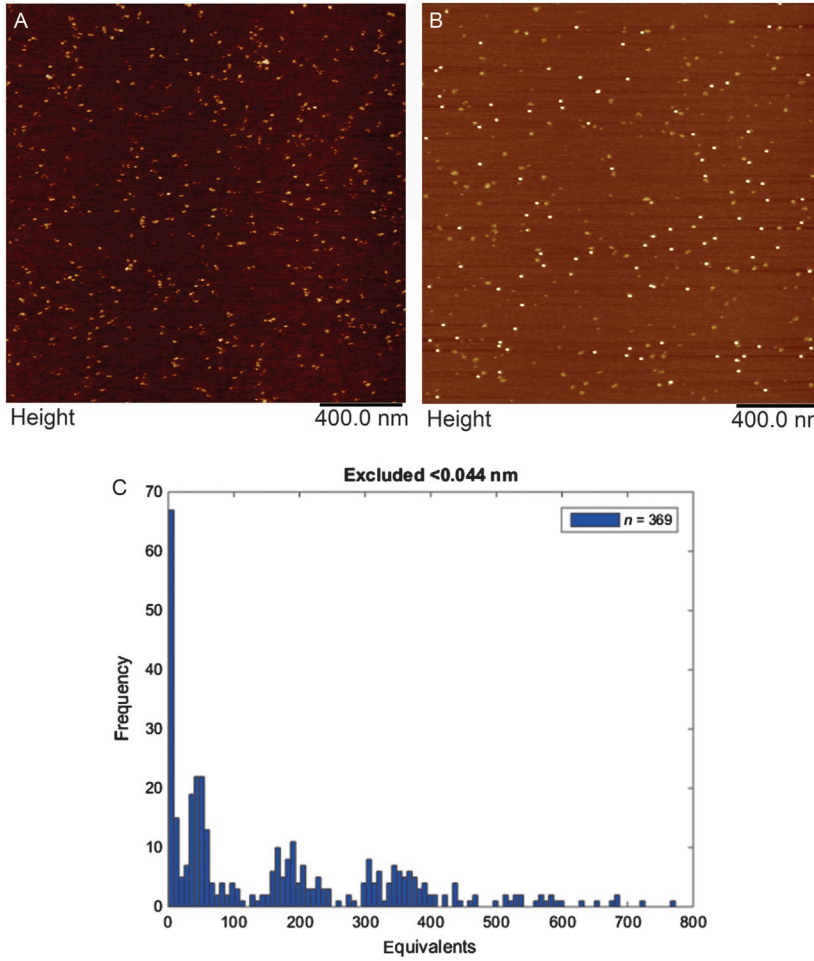

Fig. 1 Examples of effect of crowding and higher concentration on SFM imaging. (A) A crowded SFM image of Aldolase molecules. It is not possible to discern single molecules in the image. (B) SFM image of catalase at high concentration that shows multimerization. (C) Volumetric analysis of (B) using SFMedges (module of SFMetrics) showing distinct populations of multimers.

in distortions in absolute height of biomolecules (Fig. 2). Relative height is however a very reliable measurement. In experiments measuring volume it is crucial to use the same tip and system scanning parameters constant when comparing two samples (Fuentes-Perez et al., 2013). The height and width of double-stranded DNA can be used as a convenient standard for

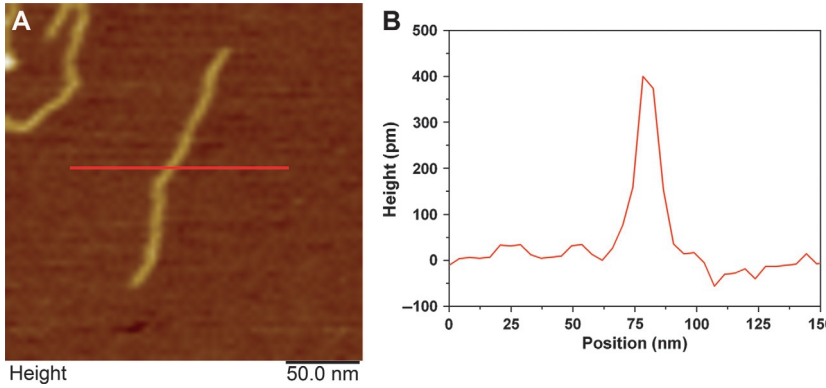

Fig. 2 Image showing the effect of convolution in SFM imaging. Note the difference in the height (~ 0.4 nm) and width (~ 12 nm) of a linear DNA molecule. Horizontal line in (A) corresponds to the cross-sectional profile shown in (B).

comparison between images. As a final note, the tip can become contaminated with material from the surface resulting in poorer image quality and requiring replacement with a new tip.

2.3 Surface Properties of the Substrate

Ideally the dynamic rearrangement of proteins, protein–protein complexes, and protein–DNA complexes required for biological function is captured during deposition for SFM imaging as a variety of conformations or architectures. This is achieved by deposition on to a suitable surface from solutions compatible with biochemical activity (or as close as practical). Sample deposition, washing and drying, is usually rapid (typically >30 s for washing and drying) to maintain distribution from solution as close as possible. A number of different substrates like mica, HOPG, glass coverslips, atomically flat gold layers, etc., have been explored for SFM imaging (Chada et al., 2015; Cisneros, Muller, Daud, & Lakey, 2006; Rahman, Neff, Green, & Norton, 2016). All of the methods described here use mica as a substrate because of its ease of use, compatibility with biochemical buffers for deposition and flatness. Mica is an aluminosilicate mineral that can easily be cleaved, using an adhesive tape, to expose an atomically flat surface. This surface has a net negative charge compatible with interaction of molecules in aqueous buffers (Maslova, Gerasimova, & Forsling, 2004). Chemical modification of the surface is not needed for the methods described here.

Chemical modification of the surface can complicate imaging and analysis as it increases surface roughness, decreasing imaging quality and it can bias the distribution of molecular conformations adhering to the surface. In addition for TIRF–SFM clarity of mica is also very important because the substrate has to be transparent in addition to being flat.

3. SFM IMAGING TO REVEAL AND QUANTIFY PROTEIN ARCHITECTURAL PLASTICITY

All proteins require flexibility for function, and the extent of flexibility varies from a few atoms at enzymatic catalytic sites to large domain reorientations needed for mechanical work. At one end of this spectrum are proteins with few or no structured element(s), designated as intrinsically disordered proteins (IDPs), where binding partners often impose structure and function are linked to the disordered-structured transitions (Uversky, 2016). The variable conformations of IDPs, and proteins with intrinsically disordered domains/regions (IDRs), make it difficult to study their structural features by methods that rely on averaging over many identical/similar molecules or complexes (i.e., X-ray crystallography, NMR, cryo-EM). Single-molecule techniques reveal structural information on individual molecules or complexes allowing different conformations or architectural arrangements to be observed and characterized. This additionally allows valuable quantification of the distribution of the different structural forms. BRCA2, for example, contains regions predicted to be intrinsically disordered thorough out the protein sequence (Sanchez et al., 2017). Indeed, SFM and TIRF–SFM have proven particularly valuable for studying BRCA2, revealing molecular plasticity, unexpected variable multimeric assemblies, and dramatic architectural reorganization upon interactions with binding partners (Sanchez et al., 2017). We describe procedures specifically for imaging and analyzing BRCA2 (general methods and some variations are described in Grosbart, Ristic, Sanchez, & Wyman, 2018).

Equipment

1. SFM capable of tapping mode operation (e.g., Multimode Nanoscope or Dimension series from Bruker or similar instrument).
2. SFM tips (e.g., Silicon Pointprobe: NHC-W, 310–371 kHz, 42 N/m from Nanosensors).

3. Standard molecular biology/biochemistry equipment for protein/DNA analysis.
4. Filtered (0.22 μm) supply of air or N_2 gas.

Buffers and Reagents

1. Sample buffer for BRCA2: 22 m*M* HEPES (pH 8.2), 2.5% glycerol, 112 m*M* NaCl, 0.12 m*M* EDTA, 0.25 m*M* DTT.
2. Deposition buffer: 10 m*M* HEPES buffer pH 8.2, 10 m*M* $MgCl_2$.
3. 1 *M* spermidine solution, filtered through a 0.22-μm filter.

Other Supplies

1. SFM sample disc: metal Ø 12 mm (e.g., from EMS or as supplied with the instrument).
2. Mica discs Ø 10 mm, Muscovite-V1 to V5 quality (from EMS). The required mica disc can be punched out of a mica sheet using a punch and die set.
3. Clear adhesive tape (e.g., 3M Scotch™ tape).
4. Strong adhesive compatible with metal surface (e.g., "super glue").
5. Lint-free wipes (e.g., Kim wipes).

Procedure

1. Thaw BRCA2 protein sample briefly on ice and dilute with HEPES sample buffer to a final composition of 10–25 ng BRCA2, 22 m*M* HEPES (pH 8.2), 2.5% glycerol, 112 m*M* NaCl, 0.12 m*M* EDTA, 0.25 m*M* DTT in a reaction volume of 20 μL.
2. Incubate sample at 37°C for 30 min without shaking.
3. Prepare substrate for sample deposition, glue mica to metal with super-glue (can be done ahead of time and kept indefinitely).
4. Cleave the mica surface by applying clear adhesive tape and pealing off to expose a clean and atomically flat surface.
5. Deposit 10–20 μL of protein sample on the mica and incubate for 1 min at room temperature.
   a. Optionally add spermidine to the sample to a concentration of 50 μ*M* before deposition. Spermidine is a polyamine and carries a positive charge, which helps in adsorption of sample to the negatively charged mica surface. In case sample adsorption appears poor, adding spermidine may increase the amount of protein absorbed.

6. After incubation, wash the sample three times (~500 μL each) with MilliQ grade water. Hold the metal disc by the edge at an angle, using a pair of tweezers, and gently add drops of water with a pipette.
7. Remove excess water by tilting the sample and blotting by the corner of a lint-free wipe.
8. Dry the sample in a gentle stream of filtered air for a minute or so until all visible water has evaporated or been blown off.
9. Mount the metal disc in the SFM and image using Tapping mode, or equivalent, according to instrument instructions.

3.1 Notes

1. A standard sample or marker with features of known dimensions (such as double-stranded DNA or protein with known dimensions at a concentration in the range of 1–5 ng/μL, or lower if the sample of interest is already fairly dense on the surface) should be included in the scanning regimen to ensure reliable images, check tip, and allow optimizing scanning parameters.
2. Lower scan rates usually provide better images. A typical feature of high scan rate is the shadowing of the particles in a flattened image.
3. For good resolution the pixel size should be smaller than the size of features of interest. Routine scan size for single-molecule imaging varies between 1×1, 2×2, and up to 5×5 μm at 512–1024 pixels per line. Larger scan size gives a better overview of the sample but lacks resolution. At 512 pixels/line or higher resolution the scan rate should be between 0.5 and 1 Hz for best images. This is balanced to be practical, based on the number of images that need to be collected, as slower scan rates increase the time to collect each image. e.g., 2×2 μm image at 512 pixels/line at 1 Hz takes about 8 min for image acquisition, while same image at 0.5 Hz takes about 15–17 min.

3.2 Image Analysis

Raw data SFM images usually have significant tilt in the nm range and, depending on the scanner, often have bowing where the edges are higher than the center. These elements of background slope are corrected by flattening the image using plane-fitting options of the image analysis software, usually standard with the instruments. The flattened images can be further analyzed by standard instrument analysis software packages, like NanoScope analysis from Bruker, JPKSPM data processing from JPK, IGOR Pro from

Asylum Research, etc., or by third party software like SPIP, Gwyddion, WSxM, Image SXM, Femtoscan online, etc. Additionally, custom scripts can be written with specific tool set for high-throughput custom image analysis. We use SFMetrics, a Matlab-based open-licensed set of routines for analysis of protein and DNA molecules (http://cluster15.erasmusmc.nl/TIRF-SFM-scripts) (Sanchez & Wyman, 2015).

3.2.1 Quantification of Molecular Structure and Architectural Features From SFM Images

Standard SFM image is a topographic or height image with Angstrom resolution in the z coordinate. Depending on the SFM instrument, additional channels of amplitude error and phase may be available as well. Because the z scale in amplitude error and phase image is not calibrated, the topographic image is the most useful for quantitative experiments with SFM. In topographic images the objects observed are defined by lateral (x, y) and height (z) measurements. This can be used to quantify size by volume and other parameters representing conformational plasticity of flexibility and irregular molecules.

3.2.2 Volumetric Analysis

SFM measured volume correlates with molecular mass, and the volume distribution of molecule in a given solution condition is a very useful parameter to measure size and consequently multimerization state (Ratcliff & Erie, 2001; Wyman et al., 1997). Volume of protein and DNA molecules can be conveniently determined, for example, by SFMetrics in a semiautomated, high-throughput manner (Sanchez & Wyman, 2015). It is often useful to also collect images of an easily identifiable protein with known volume, like RNA polymerase, as a reference to quantify multimerization of complex protein like BRCA2 (Sanchez et al., 2017). Volume of objects of interest can be determined in SFMetrics by importing an image flattened by plane-fitting as described earlier, then applying a user-defined threshold to define objects above background and sum the volume of each pixel included in the object (Sanchez & Wyman, 2015). When one threshold is applied to an entire image or image set, volumes can be determined in a high-throughput manner.

3.2.3 Conformational Flexibility

The various shapes of molecules or molecular complexes observed in SFM images are a rich source of information on conformational flexibility that can

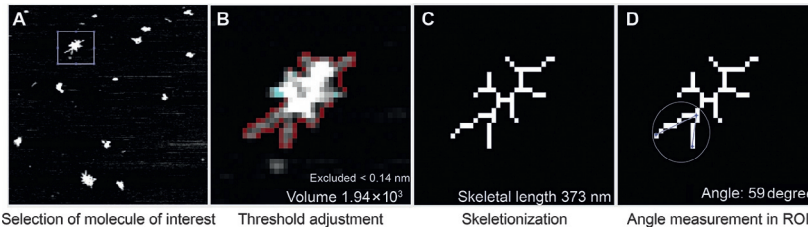

Fig. 3 Overview of conformational analysis of BRCA2 molecule by SFMetrics. (A) First the molecule of interest is selected and (B) a user-defined threshold is selected to calculate volume. (C) The molecule is skeletonized and (D) desired angles are measured.

be quantified. Standard image analysis often defines objects by the minimal oval that encloses them to provide parameters such as length (major axis), width (minor axis), and ellipticity. These standard parameters often fail to capture or accurately quantify important features of proteins and their complexes with DNA. It is important to look carefully at any image set of interest and identify the features that appear to be correlated with differences in function or conditions. Methods to quantify these often have to be developed. We have for instance observed changes in BRCA2 structure, apparent variability in condensed or extended forms, in response to different conditions that can be quantified in SFMetrics (Sanchez et al., 2017). For BRCA2 in this case we could correlate extension/compaction with different conditions by conveniently combining parameters measured in SFMetrics. Object volume was coupled to skeleton length and to angles defining arrangement of component junctions to more completely quantitatively characterize the shape of a molecule. Skeleton length measures compaction or extension of an object as the minimum number of continuous pixels needed to cover the whole structure after "skeletonization." Irregularly shaped molecules are often depicted by branched skeleton (Fig. 3), where the angle between branches can provide a robust unbiased signature of conformation.

4. SFM ANALYSIS OF RAD51 FILAMENT AND JOINT MOLECULES

As a mediator of homologous recombination BRCA2 interacts with and affects RAD51, RAD51–DNA filaments, and RAD51-mediated DNA joint molecules. To understand these interactions we will describe SFM and TIRF–SFM analysis of these multicomponent assemblies. Directly determining the arrangement of proteins and DNA in complexes representing staged steps in strand exchange during HR has proven uniquely valuable

for understanding how this process works. A family of highly conserved DNA strand exchange proteins catalyze the defining reactions of HR: homology search, strand invasion, and joint molecule formation. Our work considers the human protein, RAD51. All strand exchange proteins form nucleoprotein filaments on single-stranded DNA, which is the active complex responsible for subsequent steps of recognizing homologous sequence in a double-stranded DNA strand and catalyzing strand exchange between these two. Novel mechanistic insight into the mechanism and control of HR has been revealed from defining the arrangement of RAD51–DNA filaments correlated to reaction conditions, specific RAD51 variants or mutant forms, as well as effect of recombination mediators crucial for filament formation. Here we describe how we have applied SFM imaging to analyze filament formation, the structure of the filaments, and joint molecules. SFM imaging experiments work best when the object of interest (filaments of joint molecules) is efficiently formed and deposited while unwanted molecules/structures (excess free protein or free DNA, aggregates, etc.) are minimized. We describe here our experience with specific emphasis on aspects that are essential to allow efficient, coherent image collection while preserving authentic (biochemical) function for RAD51 filaments and joint molecules.

4.1 RAD51 Filament Formation for SFM Imaging and Analysis

Human RAD51 was expressed and purified as described (Modesti et al., 2007).

Equipment and Other Supplies

1. SFM capable of tapping mode operation (e.g., Multimode Nanoscope or Dimension series from Bruker).
2. SFM tip (e.g., Silicon Pointprobe: NHC-W, 310–371 kHz, 42 N/m from Nanosensors).
3. Standard molecular biology/biochemistry equipment for protein/DNA analysis.
4. Filtered (0.22 μm) supply of air or N_2 gas.

Buffers and Reagents

1. Reaction buffer: 25–50 m*M* HEPES or Tris–HCl pH 7.5, 2–5 m*M* $CaCl_2$, 1–2 m*M* ATP (buffered to pH 7.5), 30–50 m*M* KCl, 1 m*M* DTT.
2. Deposition buffer: 10 m*M* HEPES–KOH pH 7.5, 10 m*M* $MgCl_2$.

Procedure

1. Thaw RAD51 aliquot on ice.
2. Prepare filament formation reaction with 7.5 μ*M* DNA (bp or nucleotide concentration. Although specific length of DNA may be needed for some experiments, best results are achieved with DNA ranging from 300 to 1000 nt/bp), 2.5 μ*M* RAD51 in reaction buffer in 10 μL volume.
3. Incubate at 37°C for 10 min.
4. Dilute the reaction 3–10 times in deposition buffer, deposit 10 μL onto freshly cleaved mica, and incubate at room temperature 15 s.
5. After incubation wash mica once with about 500 μL of MilliQ water.
6. Remove excess water by tilting the sample and blotting by the corner of a lint-free wipe.
7. Dry the sample in a gentle stream of filtered air for a minute or so until all visible water has evaporated or been blown off.
8. Mount the metal disc in the SFM and image using Tapping mode, or equivalent, according to instrument instructions.

4.2 Notes

1. Optimal monovalent salt concentration for the filament formation reaction is 30–50 m*M*, which is usually contributed by protein storage buffer. If desired to make the reaction more efficient or accommodate the amount of protein needed, the concentration of monovalent salt can be adjusted to 100–200 m*M*.
2. Concentration of $CaCl_2$ is usually two times the concentration of ATP, for e.g., 2 m*M* $CaCl_2$ and 1 m*M* ATP; however, slightly higher concentrations like 5 m*M* $CaCl_2$ and 2 m*M* ATP can also be used. In these conditions stable filaments in the ATP bound form are observed. Using $MgCl_2$ or a mixture $CaCl_2$ and $MgCl_2$ allows (some) ATP hydrolysis and dynamic filaments which appear irregular with respect to arrangement and amount of protein bound.
3. The degree of dilution with deposition buffer is determined empirically for each reaction and depends to some extent on the length of DNA used. Ideally 5–10 (fewer for longer DNA, e.g., 1–2 kbp, more for shorter DNA, e.g., 200–800 bp) nonoverlapping filaments will be observed in each 2×2 μm image. It is most efficient to deposit several dilutions at once, make quick test scans, and use the one that has best distribution of molecules of interest.
4. In these conditions RAD51 forms filaments on both circular and linear DNA as well as on ss- and ds-DNA. Since filaments on circular DNA frequently collapse on themselves, linear ss- or ds-DNA is more frequently used in SFM experiments (Fig. 4).

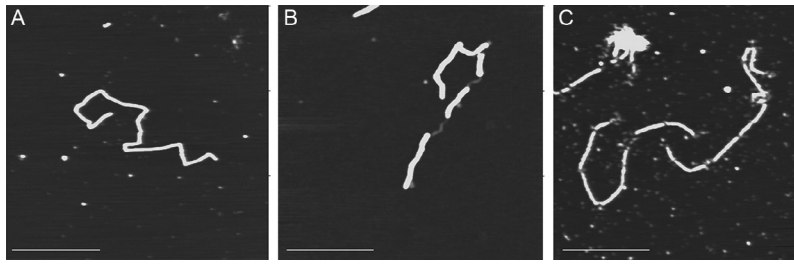

Fig. 4 Examples of RAD51 filament formation on ds-DNA substrates. (A) Regular filaments on linear ds-DNA (3901 bp). (B) Partial filament on linear ds-DNA (3901 bp). (C) Irregular filaments on linear ds-DNA (3901 bp). Scale bar 500 nm.

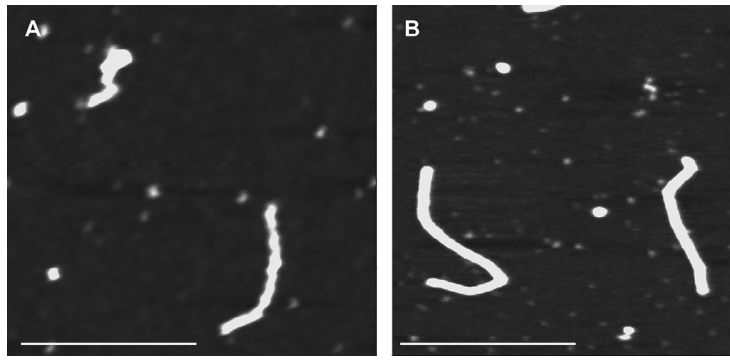

Fig. 5 Examples of RAD51 filament formation. (A) Irregular filaments on linear ss-DNA (1000 nt). (B) Regular filaments on 3′ tailed substrate (1031 nt ss- + 200 bp ds-DNA). Scale bar 500 nm.

5. Under these conditions, ATP + Ca^{2+} with 3 bp/nt DNA per monomer, RAD51 forms stable and highly regular filaments that completely cover ds-DNA. The amount of RAD51 has to be carefully titrated for each batch of protein produced. Suboptimal amounts of RAD51 result in partial filaments that tend to cluster/aggregate and complicate analysis (Fig. 4C). This undesired effect can be minimized by addition of 100 m*M* (final concentration in reaction) K_2SO_4 or $(NH_4)_2SO_4$ to the filament formation reaction with additional incubation for 10 min at 37°C before deposition. For such reaction, deposit 10 μL directly onto freshly cleaved mica without dilution with deposition buffer. On the other hand, excess protein not bound in filaments will bind to mica resulting in background roughness which can interfere with interpretation and analysis.
6. RAD51 filaments on ss-DNA tend to be more irregular. In order to produce as complete filaments as possible, excess of RAD51 protein can be used (2–1 nucleotide per monomer). Also, incubation time can be increased to 30 min. Filament formation on ss-DNA can be enhanced if the DNA is partially ds- with a ss-tail (Ristic et al., 2005) (Fig. 5).

4.3 Joint Molecule Formation

Buffers and Reagents

1. Reaction buffer: 25–50 m*M* HEPES or Tris–HCl pH 7.5, 2–5 m*M* $CaCl_2$, 1–2 m*M* ATP (buffered to pH 7.5), 30–50 m*M* KCl, 1 m*M* DTT.
2. 1 *M* K_2SO_4.
3. Wash buffer: 10 m*M* HEPES–KOH pH 7.5, 100 m*M* KCl.
4. Deposition buffer: 10 m*M* HEPES–KOH pH 7.5, 10 m*M* $MgCl_2$.

Procedure

1. Prepare filament formation reaction with 7.5 μ*M* DNA (nucleotide concentration), 2.5 μ*M* RAD51 in reaction buffer in 10 μL volume.
2. To form joint molecules prepare a reaction with 1–3 μ*M* ds-DNA (bp concentration) in reaction buffer, add 2–3 μL of the ss-DNA filament formation (from step 1) reaction to 10 μL total volume. Incubate for 15 min at 37°C.
3. Add K_2SO_4 to 100 m*M* and incubate for an additional 10 min at 37°C.
4. Deposit this reaction directly onto freshly cleaved mica and incubate for 15 s at room temperature.
5. Wash with ~500 μL of wash buffer, to remove free DNA not captured as joint molecules.
6. Remove excess water by tilting the sample and blotting by the corner of a lint-free wipe.
7. Add 10 μL deposition buffer to the mica to enable DNA to attach.
8. After 5 s, wash mica with ~500 μL of MilliQ water and dry in a filtered stream of air or N_2 gas.
9. Remove excess water by blotting with the corner of a lint-free wipe.
10. Dry the sample in a gentle stream of filtered air for a minute or so until all visible water has evaporated or been blown off.
11. Mount the metal disc in the SFM and image using Tapping mode, or equivalent, according to instrument instructions.

4.4 Notes

1. In vitro joint molecule formation is very sensitive to reaction conditions for filament formation. Filaments can be formed on ss-DNA or, with more success, on 3′-tailed substrates with partial ss- and partial ds-DNA. DNA with longer 3′ tail (1000 nt vs 300 nt) pairs more efficiently with homologous template (Wright & Heyer, 2014) (Fig. 6).

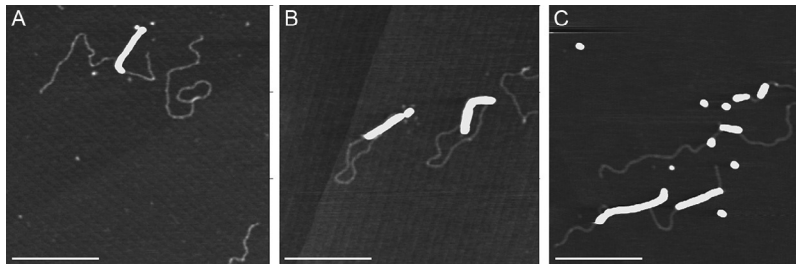

Fig. 6 Examples of joint molecule formation. (A) With linear homologous template (3901 bp) 3′ tailed substrate = 505 bp ds-region and 289 nt 3′ overhang. (B) With circular sc homologous template (3901 bp) 3′ tailed substrate = 505 bp ds-region and 289 nt 3′ overhang. (C) Difficulties in joint molecule formation if excess RAD51 ss-DNA present in filament formation reaction. Filaments formed on 3′ tailed substrate (1031 nt ss- + 200 bp ds-DNA). Template is 3901 bp ds-DNA (pDR6/XmnI). Scale bar 500 nm.

However, longer 3′ ss-DNA tail makes it challenging to form fully extended filaments.

2. The amount of RAD51 in the reaction is critical as free protein tends to bind homologous DNA template and complicates subsequent analysis. Optimal ratio for the reaction is three nucleotides or bp of DNA, in the filament formation step, per monomer of RAD51. Careful titration of each batch of RAD51 is usually required.
3. Circular as well as linear DNA can be used as the homologous ds-DNA partner. Efficiency of joint molecules formation is higher with circular DNA. If subsequent analysis will include measuring the position of joint molecule pairing, linear ds-DNA should be used. A defined position of the homologous sequence with respect to the DNA ends allows measuring parameters such as position and length of pairing (Ristic, Kanaar, & Wyman, 2011).

4.5 Analysis

To determine the effect of recombination mediators, reaction conditions or specific amino acid mutations in RAD51 on filament formation (Grigorescu et al., 2009; Holthausen et al., 2011), there are a number of parameters that can be analyzed from SFM images.

1. DNA extension upon filament formation can be determined by measuring contour length of visualized filaments. Comparison with contour length of bare DNA and RAD51 filaments on the same bp length of DNA indicates that bound DNA is extended up to 1.5 × B form length for complete continuous filaments.

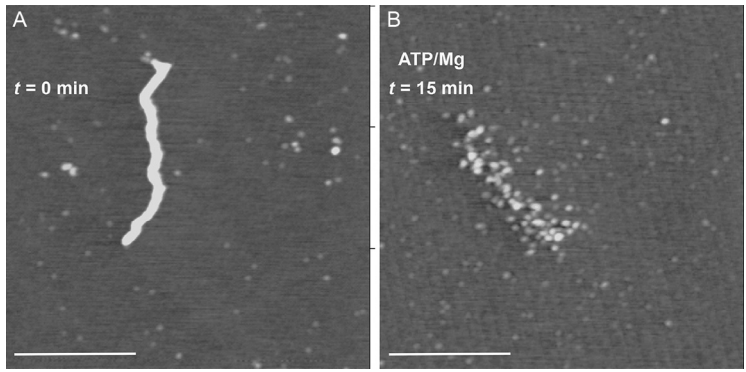

Fig. 7 Example of filament disassembly upon changing buffer conditions. (A) RAD51 filament formed on ds-DNA, 1.8 kb, in ATP + $CaCl_2$ conditions, where ATP hydrolysis is inhibited. (B) Partially disassembled RAD51 filament on ds-DNA, 1.8 kb, after buffer exchange allowing ATP hydrolysis on mica for the indicated time. Scale bar 500 nm.

2. The continuity and stiffness of filaments can also be quantified by determining the apparent persistence length of filaments based on well-known relationship between the end-to-end distance and contour length (Modesti et al., 2007).
3. Regularity or continuity of filaments is also identified by positions where protein is lacking, detected as "gaps" in the height profile or kinks in filament trajectory (Modesti et al., 2007; Ristic et al., 2011, 2005).
4. Even while immobilized on mica, RAD51 retains its ability to hydrolyze ATP and disassemble from DNA (Fig. 7). This can be analyzed by buffer exchange on mica. After deposition in conditions that do not allow ATP hydrolysis, bulk liquid is removed by wicking with a tissue from the mica edge and replaced by 10 μL of reaction buffer including ATP and $MgCl_2$. At defined time points after buffer addition and incubation at room temperature the mica is washed and dried as described earlier for SFM imaging (Ristic et al., 2005).

5. IDENTIFYING SPECIFIC PROTEINS IN COMPLEX STRUCTURES BY FLUORESCENCE: BRCA2–RAD51 COMPLEXES ANALYZED BY TIRF–SFM

Conventional SFM images as we describe here provide information on shape and size of objects but cannot identify individual specific proteins in complex structures that simply get bigger and more variable as additional components are added. However, recent advances combining SFM with

other imaging modalities (Dazzi et al., 2012; Ebenstein, Gassman, Kim, & Weiss, 2009; Sanchez et al., 2013), especially with fluorescence, can identify specific molecular constituents and provide coherent quantitative analysis of multimolecular assemblies. We have developed methods to successfully analyze the complex molecular machinery of HR. Here we describe molecular complexes of BRCA2 and RAD51, using SFM coupled to TIRF microscopy. The sample preparation for TIRF–SFM experiment is more challenging, in comparison to regular SFM. Most notably, for fluorescent imaging the sample needs to be optically transparent and for SFM atomically flat at the same time. In addition, for optimal excitation of the fluorophores from the evanescent field (generated due to total internal reflection) on a composite substrate of glass coverslip and mica, the mica layer needs to be just a few basal layers thick. However, important protein–protein and protein–DNA interaction parameters can uniquely be obtained, justifying the additional sample preparation complexity. Considering the example of BRCA2–RAD51 interaction, TIRF–SFM was used to determine the number of RAD51 molecules interacting per BRCA2 molecule under different solution conditions. In addition we determined the amount of BRCA2 and RAD51 that interact with ss-DNA in different conditions representing stages of filament formation. Sequential changes in the stoichiometry of biomolecules, interactions in a multicomponent process, can help elucidate the mechanism steps of the processes.

Full-length BRCA2 was purified as described (Jensen et al., 2010; Sanchez et al., 2017). Human RAD51 was expressed and purified as described (Modesti et al., 2007). Purified RAD51 was labeled, one fluorophore per monomer, with AF 488 at C319 using thiol maleimide chemistry. The fluorescent signal indicated the presence of RAD51, and calibrated intensity was used to determine number of monomers.

Equipment

1. SFM instrument coupled with a TIRF microscope (e.g., Nanowizard II scanner from JPK with Nikon TE 2000U microscope). In combined SFM–TIRF microscopy, it is essential that the optical and topographic image overlay with nm precision. This can be achieved by the instrument overlaying software (e.g., JPK DirectOverlay™) but requires custom workflows for more precision, such as those we have developed which provide up to 40 nm alignment accuracy (Sanchez, Kanaar, & Wyman, 2010).
2. UV lamp for curing adhesive.

Buffers and Reagents

1. Sample buffer: 12.5 m*M* HEPES pH 8.2, 4 m*M* Tris–HCl pH 7.5, 3.25% glycerol, 125 m*M* NaCl, 65 m*M* KCl, 0.4 m*M* DTT, 0.17 m*M* EDTA.
2. Deposition buffer: 10 m*M* HEPES–KCl pH 8.2, 10 m*M* $MgCl_2$.
3. 0.25% Sodium tetrahydridoborate solution (aq. w/v).
4. Fluorescent fiducial markers (e.g., 0.04 μm Ø TransFluoSpheres, 488/645, from Invitrogen).
5. Electron microscopy grade glutaraldehyde, in single use glass ampules.

Other Supplies

1. 10-mm Ø mica discs, Muscovite-V1 quality (e.g., from EMS). The required mica disc can be punched out of a mica sheet using a punch and die set.
2. 24-mm Ø clean glass coverslips, round, #0 (0.08–0.12 mm) (e.g., from Menzel-Gläser).
3. Optical adhesive (e.g., NOA88 from Norland products).
4. Clear adhesive tape (e.g., 3M Scotch™ tape).
5. Lint-free wipes (e.g., Kim wipes).

Procedure

1. Prepare mica substrate for sample deposition: For TIRF microscopy the sample should be optically transparent. This can be achieved by using an assembly of glass coverslip and thin mica. The mica discs are typically punched out of 0.15 to 0.21-mm or 0.26 to 0.31-mm thick mica sheets. Muscovite-V1 is the clearest quality of mica with no color or inclusion; however, at the supplied thickness it is too thick for TIRF microscopy.
   a. Using a scalpel tip, split the mica disc into thinner sections.
   b. Attach the thin mica disc on the glass coverslip with optical adhesive.
   c. After curing of the adhesive, cleave the mica further to make it just a few atomic layer thick. Cleaving mica to such transparency and thickness is tricky and needs practice.
   d. Next, treat the mica surface with 0.25% sodium tetrahydridoborate solution (aq. w/v) at room temperature for 20 min, to reduce background fluorescence signal. Rinse with MilliQ water.
2. Form BRCA2–RAD51 complexes by incubating 25 n*M* BRCA2 with 600 n*M* RAD51, fluorescently labeled as described (Modesti et al., 2007), in sample buffer for 30 min at 37°C.
3. Add glutaraldehyde to a final concentration of 0.12% to crosslink the protein sample and incubate for additional 5 min at 37°C.

   a. Fixation or crosslinking of the sample should be avoided as much as possible to visualize native protein–protein or protein–DNA interactions. In some cases we observe significantly reduced background for crosslinked vs noncrosslinked samples. Alternatively when potentially dynamic or short-lived reactions are to be observed, crosslinking effectively freezes a snapshot representing the mixture of molecular complexes present in a reaction.
4. Add 50 m*M* Tris–HCl pH 7.5 to quench excess glutaraldehdye.
5. Dilute sample 20–200 times in deposition buffer to reduce background fluorescence from free RAD51.
6. Add 3 p*M* TranFluospheres fiducial markers.
7. Deposit 20 μL of this sample on the prepared mica substrate. Adsorb for 1 min. Rinse the mica with about 1 mL of MilliQ water and dry in stream of filtered air. Image with TIRF–SFM (see Fig. 8 for schematic overview of TIRF–SFM work flow).
8. Obtain a TIRF optical image of the fluorescent signal at wavelength appropriate for imaging the fiducials.
9. Obtain a TIRF optical image of the fluorescent signal at a wavelength appropriate for imaging the sample. We typically collect a stack of exposures from this sample field, 300 frames, each as 300 ms exposures.
10. Collect SFM topographic image of the same area.

5.1 Tips for SFM–TIRF Imaging

1. Optimal density of the sample is crucial for reliable TIRF–SFM data. While SFM provides nanometer resolution, TIRF resolution is diffraction limited. Therefore, the (fluorescent) proteins or complexes must be distributed so that their fluorescent signals do not overlap. Typically molecules should be >250 nm apart (Fig. 9).
2. Large scan sizes (e.g., 35×35 μm) provide optimal overlay of SFM and TIRF images.
3. To maintain high resolution in terms of pixel size and slow scan rate for good image quality. We have best success collecting such large topographic images overnight.
4. There should be at least three fiducial markers in a given field of view for precise alignment of fluorescence and SFM image (Fig. 10).

5.2 Notes

1. NOA 88 cures at long wavelength UV light (315–395 nm) with an optimum at 365 nm.
2. There should be no air bubbles between the mica and the glass coverslip.

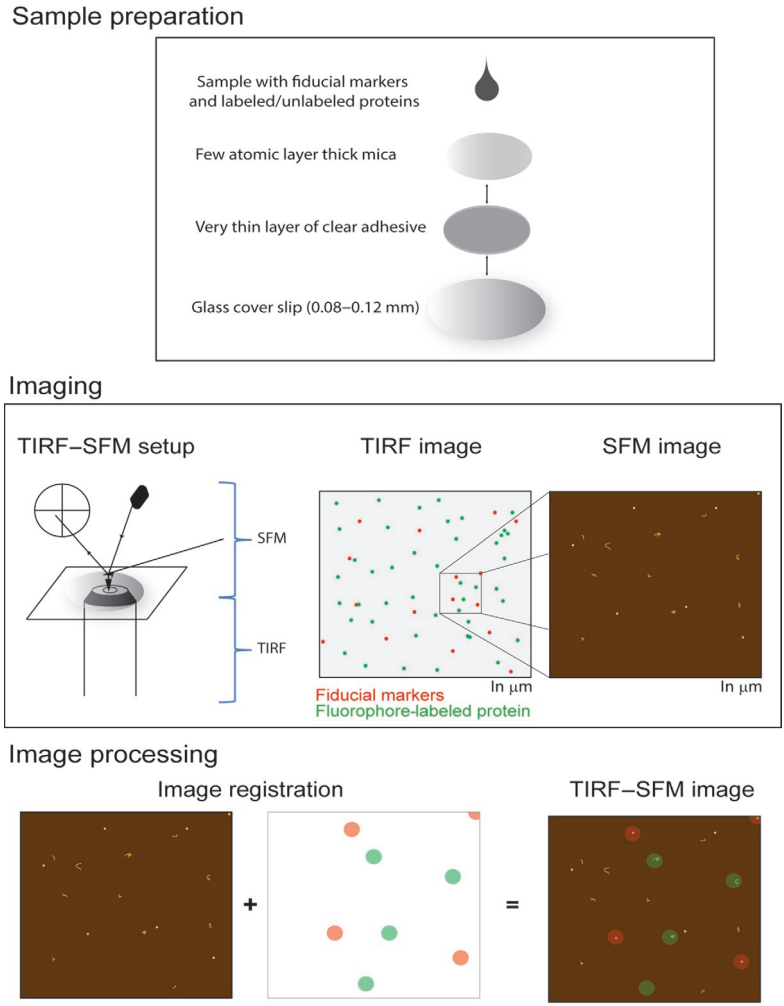

Fig. 8 Overview of steps in experiments applying TIRF–SFM imaging. Schematic representation of sample preparation steps, image collection aspects, and required post collection image processing to create merged fluorescent and topographic data.

3. The excitation wavelength of the sample fluorophore and the fiducial markers should not overlap to avoid photobleaching of the sample while focusing.
4. Obtaining large size scans at high resolution require several hours to overnight to collect. A microscopy environment that limits vibrations and noise is required.

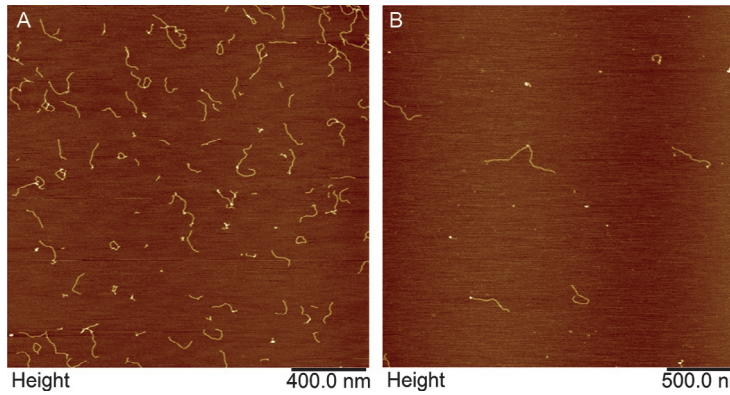

Fig. 9 Representative image, example of DNA molecules, comparing optimal mica coverage for (A) SFM and (B) TIRF–SFM imaging where molecules/complexes with potential fluorescent signals have to be separated by >200 nm.

5.3 Image Analysis and Quantification

Analysis of the TIRF–SFM data requires the following general steps: Locate the position of the fiducials and the sample from the fluorescence signals, register TIRF and SFM images, and quantify the amount of fluorescence for each ROI (for detailed description, see Sanchez et al., 2013). The topographic SFM image can be used to analyze objects with respect their size and shape as described in previous sections. The addition of fluorescence localization and fluorescence intensity adds considerable functional information for multicomponent complexes such as BRCA2–RAD51. We have used this to analyze the role of BRCA2 in setting up RAD51 filaments in collaboration with other HR proteins for eventual DNA strand exchange.

1. Determine the locations of each fluorescent signal (ROI) by accumulating the signal from sets of 10 consecutive frames, (3 s total exposure time) in a single frame; repeat for frames 2–11, etc., until all frames have been accounted for.
2. From each ROI, the position is calculated by fitting the fluorescent signal, summed over 10 frames, with a two-dimensional Gaussian function (nonlinear least-squares method) to determine the mean of this intensity distribution. This operation is repeated with the next 10 consecutive frames until last frame acquired, generating a cloud of positions per ROI. Finally, from each ROI, both from the fiducials and sample, the centroid of the cluster can be estimated from a normal fitting.
3. Register TIRF and SFM images by matching the "optical" centroid with the "topographic" center of mass of the fiducials (Fig. 10). This will produce a matrix with the scaling (S) and translation factor (T) needed for the sample.

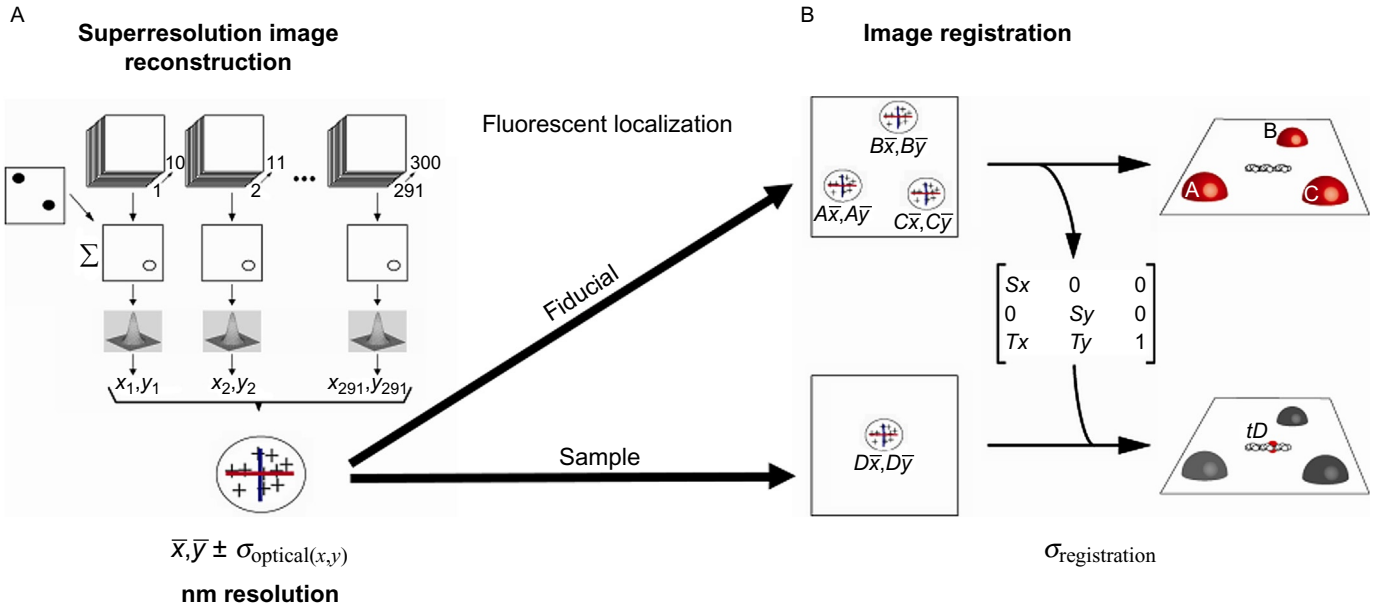

Fig. 10 Flowchart illustrating steps in TIRF–SFM image processing for registration and eventual analysis. (A)The fluorescent signals coming from the fiducials and the sample are separately processes (collected a different wavelength). The *X*–*Y* coordinates of the fluorescent source is calculated from point spread function from sum of 10 frames, and uncertainty determined for this localization based on the cloud as indicated in the summed image large "+" sign (vertical = uncertainly in *Y* and horizontal = uncertainty in *X*). (B) The location of the fiducials as determined in (A) is mapped onto their topographic center of mass (objects labeled A, B, and C) to create transformation matrix which is applied to the sample fluorescent localization to determine their position with respect to the sample topographic image (object labeled D).

4. Quantify the number of fluorophores per ROI based on stepwise photobleaching, calibrated by the signal from a single fluorophores:
   a. Correct individual frames for background and select ROIs.
   b. Extract from each ROI the intensity (N) trace over time.
   c. Variations in intensity can be estimated with a step fitting algorithm (Kerssemakers et al., 2006; van Mameren et al., 2009) and the intensity of a single fluorophore defined as the average step size for each ROI. This number (ΔN) divided by the maximum N in the ROI represents the number of fluorophores. It is useful to calibrate this type of measurement with objects with a known number of fluorophores, for example, a stoichiometrically labeled protein(complex) defined by size based on SFM volume.

6. CONCLUSIONS

SFM-based approaches provide unique information probing the nanoscale properties of biomolecules. Most importantly they help to bridge the gap between the atomic resolution structural studies and the cell-based microscopic studies. Because only low concentrations of proteins are needed, SFM is an indispensable practical tool to study hard to purify proteins and their complexes. In addition the advantage of observing, categorizing, and quantifying all examples in a sample reveals conformational plasticity and multimerization under various conditions. SFM-based approaches have also been especially useful in elucidating DNA protein interactions for complex multistep biological processes like HR repair. Stoichiometry and assembly–disassembly of proteins into DNA-based multimolecular complexes can be accurately investigated by staging reactions based on biochemically defined conditions. Fluorescence-coupled SFM in TIRF mode allows identifying one or more protein molecule(s) with fluorescent dyes thus combining the versatility of fluorescence with accuracy and ease of SFM to study molecular reactions at single-molecule resolution.

REFERENCES

Chada, N., Sigdel, K. P., Gari, R. R., Matin, T. R., Randall, L. L., & King, G. M. (2015). Glass is a viable substrate for precision force microscopy of membrane proteins. *Scientific Reports*, *5*, 12550. https://doi.org/10.1038/srep12550.

Cisneros, D. A., Muller, D. J., Daud, S. M., & Lakey, J. H. (2006). An approach to prepare membrane proteins for single-molecule imaging. *Angewandte Chemie (International Edition in English)*, *45*(20), 3252–3256. https://doi.org/10.1002/anie.200504506.

Dazzi, A., Prater, C. B., Hu, Q., Chase, D. B., Rabolt, J. F., & Marcott, C. (2012). AFM-IR: Combining atomic force microscopy and infrared spectroscopy for nanoscale chemical characterization. *Applied Spectroscopy*, *66*(12), 1365–1384. https://doi.org/10.1366/12-06804.

Ebenstein, Y., Gassman, N., Kim, S., & Weiss, S. (2009). Combining atomic force and fluorescence microscopy for analysis of quantum-dot labeled protein-DNA complexes. *Journal of Molecular Recognition*, *22*(5), 397–402. https://doi.org/10.1002/jmr.956.

Fuentes-Perez, M. E., Dillingham, M. S., & Moreno-Herrero, F. (2013). AFM volumetric methods for the characterization of proteins and nucleic acids. *Methods*, *60*(2), 113–121. https://doi.org/10.1016/j.ymeth.2013.02.005.

Grigorescu, A. A., Vissers, J. H., Ristic, D., Pigli, Y. Z., Lynch, T. W., Wyman, C., et al. (2009). Inter-subunit interactions that coordinate Rad51's activities. *Nucleic Acids Research*, *37*(2), 557–567. https://doi.org/10.1093/nar/gkn973.

Grosbart, M., Ristic, D., Sanchez, H., & Wyman, C. (2018). Imaging of DNA and protein by SFM and combined SFM-TIRF microscopy. *Methods in Molecular Biology*, *1665*, 259–280. https://doi.org/10.1007/978-1-4939-7271-5_14.

Holthausen, J. T., van Loenhout, M. T., Sanchez, H., Ristic, D., van Rossum-Fikkert, S. E., Modesti, M., et al. (2011). Effect of the BRCA2 CTRD domain on RAD51 filaments analyzed by an ensemble of single molecule techniques. *Nucleic Acids Research*, *39*(15), 6558–6567. https://doi.org/10.1093/nar/gkr295.

Jensen, R. B., Carreira, A., & Kowalczykowski, S. C. (2010). Purified human BRCA2 stimulates RAD51-mediated recombination. *Nature*, *467*(7316), 678–683. https://doi.org/10.1038/nature09399.

Kerssemakers, J. W., Munteanu, E. L., Laan, L., Noetzel, T. L., Janson, M. E., & Dogterom, M. (2006). Assembly dynamics of microtubules at molecular resolution. *Nature*, *442*(7103), 709–712. https://doi.org/10.1038/nature04928.

Kolinjivadi, A. M., Sannino, V., de Antoni, A., Techer, H., Baldi, G., & Costanzo, V. (2017). Moonlighting at replication forks—A new life for homologous recombination proteins BRCA1, BRCA2 and RAD51. *FEBS Letters*, *591*(8), 1083–1100. https://doi.org/10.1002/1873-3468.12556.

Maslova, M. V., Gerasimova, L. G., & Forsling, W. (2004). Surface properties of cleaved mica. *Colloid Journal*, 66(3), 322–328. https://doi.org/10.1023/B:COLL.0000030843.30563.c9.

Mehta, A., & Haber, J. E. (2014). Sources of DNA double-strand breaks and models of recombinational DNA repair. *Cold Spring Harbor Perspectives in Biology*, *6*(9), a016428. https://doi.org/10.1101/cshperspect.a016428.

Modesti, M., Ristic, D., van der Heijden, T., Dekker, C., van Mameren, J., Peterman, E. J., et al. (2007). Fluorescent human RAD51 reveals multiple nucleation sites and filament segments tightly associated along a single DNA molecule. *Structure*, *15*(5), 599–609. https://doi.org/10.1016/j.str.2007.04.003.

Moreno-Herrero, F., de Jager, M., Dekker, N. H., Kanaar, R., Wyman, C., & Dekker, C. (2005). Mesoscale conformational changes in the DNA-repair complex Rad50/Mre11/Nbs1 upon binding DNA. *Nature*, *437*(7057), 440–443. https://doi.org/10.1038/nature03927.

Prakash, R., Zhang, Y., Feng, W., & Jasin, M. (2015). Homologous recombination and human health: The roles of BRCA1, BRCA2, and associated proteins. *Cold Spring Harbor Perspectives in Biology*, 7(4), a016600. https://doi.org/10.1101/cshperspect.a016600.

Rahman, M., Neff, D., Green, N., & Norton, M. L. (2016). DNA origami reorganizes upon interaction with graphite: Implications for high-resolution DNA directed protein patterning. *Nanomaterials (Basel)*, *6*(11), E196. https://doi.org/10.3390/nano6110196.

Ratcliff, G. C., & Erie, D. A. (2001). A novel single-molecule study to determine protein–protein association constants. *Journal of the American Chemical Society*, *123*(24), 5632–5635. https://doi.org/10.1021/ja005750n.

Ristic, D., Kanaar, R., & Wyman, C. (2011). Visualizing RAD51-mediated joint molecules: Implications for recombination mechanism and the effect of sequence heterology. *Nucleic Acids Research*, *39*(1), 155–167. https://doi.org/10.1093/nar/gkq766.

Ristic, D., Modesti, M., van der Heijden, T., van Noort, J., Dekker, C., Kanaar, R., et al. (2005). Human Rad51 filaments on double- and single-stranded DNA: Correlating regular and irregular forms with recombination function. *Nucleic Acids Research*, *33*(10), 3292–3302. https://doi.org/10.1093/nar/gki640.

Sanchez, H., Kanaar, R., & Wyman, C. (2010). Molecular recognition of DNA-protein complexes: A straightforward method combining scanning force and fluorescence microscopy. *Ultramicroscopy*, *110*(7), 844–851. https://doi.org/10.1016/j.ultramic.2010.03.002.

Sanchez, H., Kertokalio, A., van Rossum-Fikkert, S., Kanaar, R., & Wyman, C. (2013). Combined optical and topographic imaging reveals different arrangements of human RAD54 with presynaptic and postsynaptic RAD51-DNA filaments. *Proceedings of the National Academy of Sciences of the United States of America*, *110*(28), 11385–11390. https://doi.org/10.1073/pnas.1306467110.

Sanchez, H., Paul, M. W., Grosbart, M., van Rossum-Fikkert, S. E., Lebbink, J. H. G., Kanaar, R., et al. (2017). Architectural plasticity of human BRCA2-RAD51 complexes in DNA break repair. *Nucleic Acids Research*, *45*(8), 4507–4518. https://doi.org/10.1093/nar/gkx084.

Sanchez, H., & Wyman, C. (2015). SFMetrics: An analysis tool for scanning force microscopy images of biomolecules. *BMC Bioinformatics*, *16*, 27. https://doi.org/10.1186/s12859-015-0457-8.

Shahid, T., Soroka, J., Kong, E. H., Malivert, L., McIlwraith, M. J., Pape, T., et al. (2014). Structure and mechanism of action of the BRCA2 breast cancer tumor suppressor. *Nature Structural and Molecular Biology*, *21*(11), 962–968. https://doi.org/10.1038/nsmb.2899.

Stracker, T. H., Theunissen, J. W., Morales, M., & Petrini, J. H. (2004). The Mre11 complex and the metabolism of chromosome breaks: The importance of communicating and holding things together. *DNA Repair (Amst)*, *3*(8–9), 845–854. https://doi.org/10.1016/j.dnarep.2004.03.014.

Thorslund, T., McIlwraith, M. J., Compton, S. A., Lekomtsev, S., Petronczki, M., Griffith, J. D., et al. (2010). The breast cancer tumor suppressor BRCA2 promotes the specific targeting of RAD51 to single-stranded DNA. *Nature Structural and Molecular Biology*, *17*(10), 1263–1265. https://doi.org/10.1038/nsmb.1905.

Uversky, V. N. (2016). p53 proteoforms and intrinsic disorder: An illustration of the protein structure-function continuum concept. *International Journal of Molecular Sciences*, *17*(11), E1874. https://doi.org/10.3390/ijms17111874.

van Gent, D. C., Hoeijmakers, J. H., & Kanaar, R. (2001). Chromosomal stability and the DNA double-stranded break connection. *Nature Reviews. Genetics*, *2*(3), 196–206. https://doi.org/10.1038/35056049.

van Mameren, J., Modesti, M., Kanaar, R., Wyman, C., Peterman, E. J., & Wuite, G. J. (2009). Counting RAD51 proteins disassembling from nucleoprotein filaments under tension. *Nature*, *457*(7230), 745–748. https://doi.org/10.1038/nature07581.

van Raaij, M. E., Segers-Nolten, I. M., & Subramaniam, V. (2006). Quantitative morphological analysis reveals ultrastructural diversity of amyloid fibrils from alpha-synuclein mutants. *Biophysical Journal*, *91*(11), L96–98. https://doi.org/10.1529/biophysj.106.090449.

Wright, W. D., & Heyer, W. D. (2014). Rad54 functions as a heteroduplex DNA pump modulated by its DNA substrates and Rad51 during D loop formation. *Molecular Cell*, *53*(3), 420–432. https://doi.org/10.1016/j.molcel.2013.12.027.

Wyman, C., Rombel, I., North, A. K., Bustamante, C., & Kustu, S. (1997). Unusual oligomerization required for activity of NtrC, a bacterial enhancer-binding protein. *Science*, *275*(5306), 1658–1661.

Yang, H., Jeffrey, P. D., Miller, J., Kinnucan, E., Sun, Y., Thoma, N. H., et al. (2002). BRCA2 function in DNA binding and recombination from a BRCA2-DSS1-ssDNA structure. *Science*, *297*(5588), 1837–1848. https://doi.org/10.1126/science.297.5588.1837.

Yang, H., Li, Q., Fan, J., Holloman, W. K., & Pavletich, N. P. (2005). The BRCA2 homologue Brh2 nucleates RAD51 filament formation at a dsDNA-ssDNA junction. *Nature*, *433*(7026), 653–657. https://doi.org/10.1038/nature03234.

Yang, G. L., Vesenka, J. P., & Bustamante, C. J. (1996). Effects of tip-sample forces and humidity on the imaging of DNA with a scanning force microscope. *Scanning*, *18*(5), 344–350.